Elias R. Melhem, MD
Ryuta Itoh, MD, PhD
Paul J. M. Folkers, PhD

Abbreviations:
CSF = cerebrospinal fluid
ES = echo spacing
SE = spin echo
SI = signal intensity
TF = turbo factor
TF × ES = number of echoes per TR multiplied by the time between echoes
TR = repetition time
TR − (TF × ES) = time available for recovery of longitudinal magnetization
3D = three-dimensional

Cervical Spine: Three-dimensional Fast Spin-Echo MR Imaging—Improved Recovery of Longitudinal Magnetization with Driven Equilibrium Pulse[1]

At magnetic resonance (MR) imaging of the cervical spine, pulse sequences that provide high signal from cerebrospinal fluid (CSF) (myelographic effect) help delineate epidural pathologic processes, such as disk fragments and osteophytes. On the basis of computer simulations that account for the effect of the driven equilibrium pulse on steady-state magnetization, the authors evaluated a three-dimensional fast spin-echo MR imaging technique that provides hyperintense CSF. At MR imaging of the cervical spine in five adult human volunteers, the pulse sequence was found to be time efficient and nearly isotropic. Magnetic resonance (MR) imaging of the cervical spine for evaluation of disk herniation and spondylosis remains challenging despite advances in hardware design and innovations in pulse sequence development (1,2). Time-efficient pulse sequences that provide high-spatial-resolution MR images with hyperintense cerebrospinal fluid (CSF) (myelographic effect) are desirable for the evaluation of the degenerated cervical spine (3,4). Further, these pulse sequences preferably should have low sensitivity to physiologic and nonphysiologic motion-related and susceptibility artifacts (5–10).

Fast spin-echo (SE)– and gradient-echo–based three-dimensional (3D) MR imaging techniques are being refined continuously for imaging of the cervical spine (11–14). Gradient-echo techniques, spoiled or steady state, provide fast high-spatial-resolution MR imaging of the cervical spine with a consistent myelographic effect. The major disadvantage of these

techniques is high sensitivity to susceptibility differences (9,10). On the other hand, 3D fast SE techniques are appreciably less sensitive to susceptibility artifacts owing to multiple refocusing 180° radio-frequency pulses (turbo factor [TF]) and short echo spacing (ES). The disadvantages of these techniques include relatively long imaging times for comparable spatial resolution and inconsistent myelographic effect despite gradient moment nulling (11). Two methods for improving the efficiency of 3D fast SE MR imaging are shortening of the repetition time (TR) and increasing of the echo train length. The former method increases T1 weighting, which degrades the myelographic effect, and the latter results in blurring artifacts from T2-decay–induced modulations in the amplitude of the echo in k space (15).

A modification recently applied to fast SE techniques, known as "driven equilibrium," shows potential for preservation of the myelographic effect at very short TRs (16,17). Driven equilibrium consists of application of a resonant 90° radio-frequency pulse precisely at the time when the transverse magnetization is refocused by the last SE 180° radio-frequency pulse and properly adjusted field gradients. This driven equilibrium pulse transforms the residual transverse magnetization (long T2) of CSF into longitudinal magnetization (Fig 1). This artificial improvement in longitudinal magnetization recovery of CSF obviates long TR to achieve the myelographic effect.

On the basis of computer simulations that account for the effect of the driven equilibrium pulse on steady-state magne-

tization and guided by acquisition time considerations, we developed a time-efficient (211-msec TR) nearly isotropic 3D fast SE technique. The purpose of this study was to evaluate the ability of this technique to provide high-spatial-resolution MR images of the cervical spine with hyperintense CSF (myelographic effect).

▌ Materials and Methods

Theoretic Analysis

van Uijen and Den Boef (16) derived the equation to quantify the effect of the driven equilibrium pulse on steady-state signal intensity (SI) at the time of echo sampling. We modified this equation to account for the multiecho readout (fast SE):

$$SI = kM_o/\{1 + [T1/T2][TF \times ES]$$
$$\div [TR - (TF \times ES)]\},$$

where k and M_o represent instrumental parameters and proton density, respectively (16), and TF $\times$ ES is the number of echoes per TR multiplied by the time between echoes. With this equation, SI from CSF and cord were generated as a function of TF $\times$ ES (0–190 msec by increments of 10 msec) for different TRs (200, 300, 400, and 500 msec). Approximate T1 and T2, respectively, of CSF (4,200 and 2,100 msec) and cord (745 and 95 msec) were used in the calculations (18). The instrumental parameters were assumed to be fixed and were assigned a normalized value of 1, and the proton density was normalized relative to CSF so that the proton density of the cord was 0.7.

Myelographic contrast ($SI_{CSF} - SI_{cord}$) was plotted versus TF $\times$ ES for the different TRs. Next, the acquisition time of a 3D fast SE sequence, designed to image the cervical spine in the sagittal plane, was determined at the MR imaging console (ACS NT Power Trak 6000; Philips Medical Systems, Shelton, Conn) for different TFs and TRs. The pulse sequence was fixed for effective echo time (60 msec), spatial resolution (~1-mm³ voxel), and coverage (70 partitions).

The computer-generated simulations of myelographic contrast and acquisition time helped in the choice of pulse parameters (specifically, TR and TF) for cervical spine imaging in volunteers.

MR Imaging Technique

All MR imaging was performed with the 1.5-T superconducting magnet with peak amplitude gradient of 23 mT $\cdot$ m^{-1}
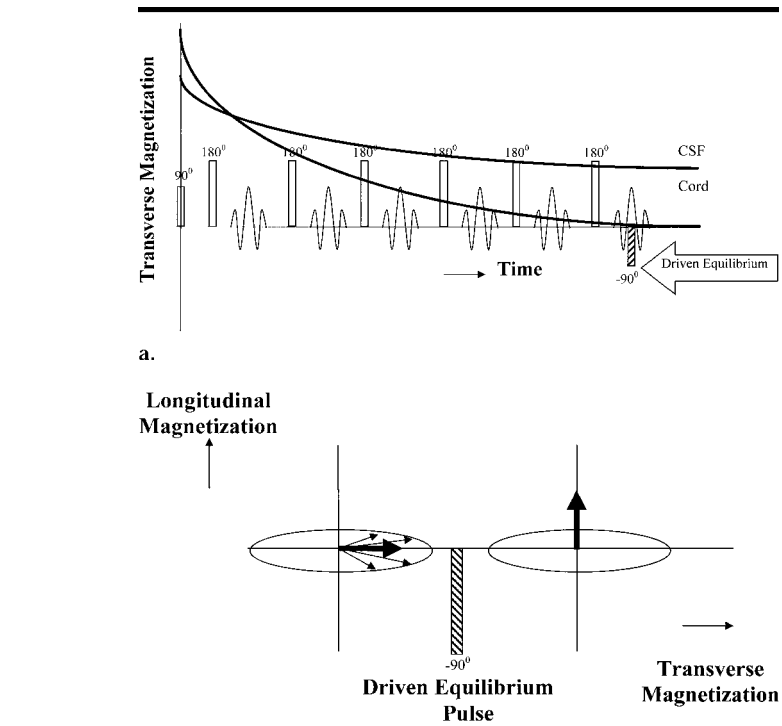

Figure 1. (a) Schematic depicts the fast SE MR imaging pulse sequence with the driven equilibrium pulse applied at the time of the last echo. (b) Schematic depicts transformation of the residual transverse magnetization to longitudinal magnetization by means of the driven equilibrium pulse.

and maximum slew rate of 103 mT $\cdot$ m^{-1} $\cdot$ msec^{-1}. The imager was operated with software version 6.0 supplemented by a research patch file (Maya 1; Philips Medical Systems, Best, the Netherlands) that provided the driven equilibrium pulse option. MR images of the cervical spine were obtained with a quadrature neck coil operating in receive mode.

Human Volunteer Study

Institutional review board approval and informed consent from the volunteers were obtained before the beginning of the study.

On the basis of results with computer-generated simulations, five volunteers (three men, two women; age range, 31–40 years; mean age, 35 years) underwent imaging in the sagittal plane with a 3D MR sequence with a short TR (211 msec) with and without application of the driven equilibrium pulse. Four of the five volunteers had known degenerative disease of the cervical spine and were specifically asked to participate in the study. The remaining volunteer had no disease related to the cervical spine. The parameters of the pulse sequence were repetition time msec/echo time msec [effec-

tive] of 211/60, TF of 16, ES of 7.1 msec, two signals acquired, and readout bandwidth of 733 Hz per pixel. One 70-mm-thick slab was partitioned into 70 2-mm-thick partitions that were reduced to an effective thickness of 1 mm by means of interpolation (zero filling). The field of view was 256 mm (60% rectangular), and the imaging matrix was 256 × 256, giving an in-plane spatial resolution of 1 × 1 mm. First-order gradient moment nulling was applied in the superoinferior direction. The acquisition time was 4 minutes 14 seconds. Subsequently, 1-mm-thick transverse reformatted MR images of the entire cervical spine were generated at the MR imager console.

The pulse sequence parameters were chosen for the following reasons. (a) Nearly isotropic voxels would allow transverse reformatted MR images with sufficient spatial resolution for evaluation of spondylotic changes. (b) Short TR would allow efficient 3D MR imaging of the cervical spine with sufficient coverage. (c) The long echo train relative to the short TR would maximize loss of transverse magnetization (T2 decay) and minimize the time available (TR − [TF × ES]) for recovery of longitudinal magnetiza-
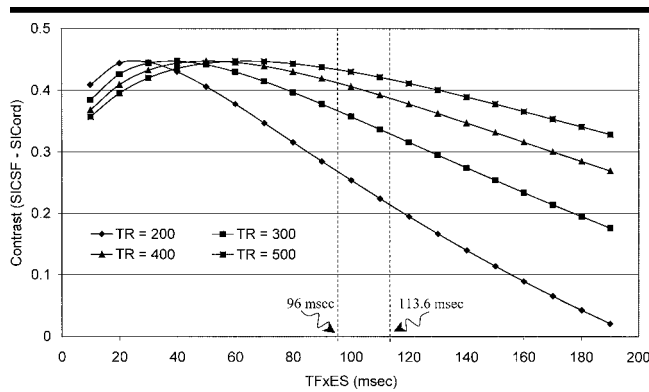
Figure 2. Computer-generated scatterplots of contrast versus TF × ES for different TRs. The peak contrast (0.45) generated by the driven equilibrium pulse is independent of TR but occurs at longer values of TF × ES (left shift) as the TR is increased from 200 to 500 msec. The range of TF × ES values (96.0–113.6 msec, dashed lines) is dictated by the choice of sequence parameters.

TABLE 1
Acquisition Times at Different TR and TF × ES Values for 3D Fast SE MR Imaging of the Cervical Spine at Fixed Spatial Resolution (~1-mm³ voxel) and Effective Echo Time (60 msec)

			Acquisition Time (min:sec)			
TF	ES (msec)	TF × ES (msec)	TR of 500 msec	TR of 400 msec	TR of 300 msec	TR of 200 msec
16	7.1	113.6	10:00	8:00	6:00	4:14
14	8.0	112.0	11:03	8:50	6:38	4:40
12	9.2	110.4	13:09	10:31	7:54	5:34
10	10.9	109.0	15:46	12:37	9:28	6:40
8	13.3	106.4	19:58	15:59	11:59	8:26
6	17.1	102.6	26:16	21:01	15:46	11:06
4	24.0	96.0	35:56	31:56	23:57	16:51

tion (T1) of non-CSF components of the cervical spine.

The sagittal MR images of the cervical spine obtained without and with application of the driven equilibrium pulse and their corresponding transverse reformatted MR images were qualitatively evaluated by an experienced neuroradiologist (E.R.M.) who was not blinded to the MR imaging parameters. The evaluation included contrast characteristics of the different components of the cervical spine (cord, CSF, vertebrae, ligaments, and intervertebral disks) and the contrast and sharpness of the CSF-cord interface. The lowest representative grade was recorded on the basis of a previously established scale (3): 1, CSF isointense with and indistinguishable from cord; 2, CSF slightly hyperintense relative to cord; 3, hyperintense CSF with indistinct cord contour; and 4, hyperintense CSF and sharply defined cord margin.

SI was measured in regions of interest placed in the CSF, spinal cord, disk, and bone marrow. The regions of interest var-

ied in size and shape for the different anatomic locations in the cervical spine (CSF, spinal cord, disk, and bone marrow) but were identical for the same anatomic location across subjects. The size of the regions of interest ranged from 10.8 to 35.4 mm². The SD of the mean SI of air was used to estimate noise.

Results

Theoretic Analysis

Plots of contrast ($SI_{CSF} - SI_{cord}$) versus TF × ES demonstrated that the driven equilibrium pulse could generate myelographic contrast at all tested values of TF × ES and TR. The peak myelographic effect (peak $SI_{CSF} - SI_{cord} = 0.45$) was independent of TR but occurred at longer values of TF × ES (right shift) as the TR was increased from 200 to 500 msec (Fig 2). Acquisition time with the 3D fast SE MR imaging sequence increased with TR and decreased with TF (Table 1).

Our choice of sequence parameters,

particularly the filling of linear k space in the phase direction and effective echo time, limited the maximum TF to 16 and the range of TF × ES from 96.0 to 113.6 msec. At this range of TF × ES values, the peak myelographic effect could not be achieved with any of the tested TRs. However, the myelographic effect was maximized at TR of 500 msec (Fig 2). This resulted in a conflict between optimization of imaging efficiency and achievement of maximum myelographic contrast. In the volunteer study, we opted for the highest imaging efficiency (shortest TR and maximum allowable TF) at the expense of optimization of myelographic contrast.

Human Volunteer Study

For all five volunteers, grading of the contrast and sharpness of the CSF-cord interface on both the sagittal and transverse reformatted MR images of the cervical spine improved from 1 to 4 with application of the driven equilibrium pulse (Fig 3). This improvement persisted even at levels of moderate to severe central stenosis (Fig 4).

After application of the driven equilibrium pulse, the mean CSF signal-to-noise ratio increased by a factor of 4.75, whereas the mean signal-to-noise ratios of cord, disk, and bone marrow decreased by a factor of 0.86, 0.76, and 0.84, respectively (Table 2). The contrast-to-noise ratio ($[SI_{CSF} - SI_{cord}]$/noise) increased from -3.89 (no myelographic effect) to 62.6 (strong myelographic effect).

The sagittal and reformatted transverse MR images of the cervical spine demonstrated complex contrast characteristics. The appearance of vertebrae, ligaments, and intervertebral disks was typical for T1-weighted images, and the hyperintense CSF was suggestive of T2 weighting. Hydrated disks were hypointense to vertebrae, and contrast between exiting nerve roots and surrounding tissues in the neural foramina was limited (Fig 3).

Discussion

In the cervical spine, MR pulse sequences that provide high signal from CSF (myelographic effect) help delineate epidural pathologic processes, such as disk fragments and osteophytes (3,4).

On MR images, SI for the different components of the cervical spine is determined by steady-state longitudinal and transverse magnetization. Fast SE readouts can influence these steady-state
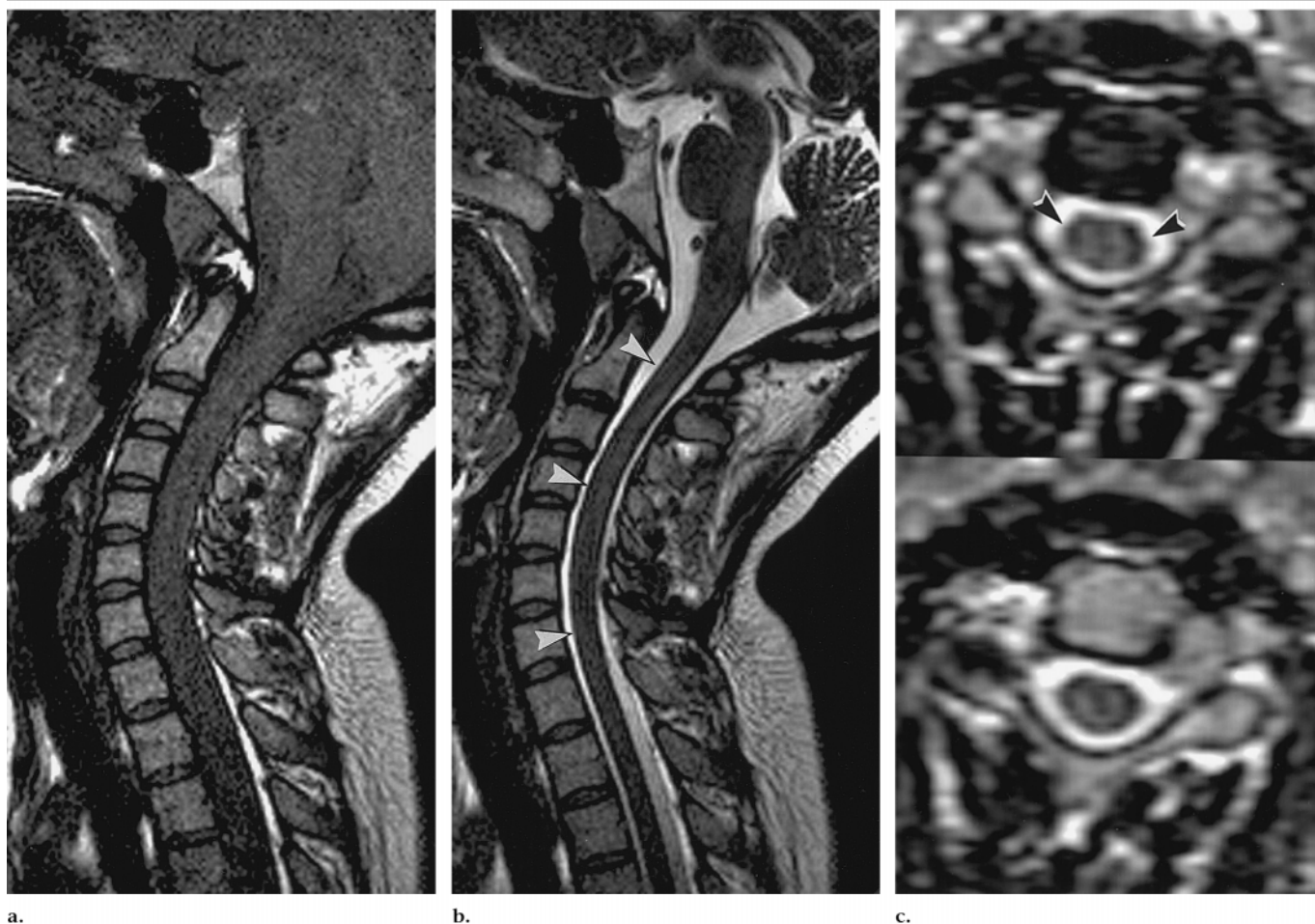
Figure 3. No degenerative disease of the cervical spine in a 26-year-old female volunteer. **(a, b)** Sagittal 3D fast SE (211/60 [effective]) MR images of the cervical spine were acquired **(a)** without and **(b)** with the driven equilibrium pulse. In **b**, the contrast and sharpness of the CSF-cord interface (arrowheads) improve from grade 1 to grade 4. **(c)** Transverse 1-mm-thick contiguous reformatted MR images were obtained at the C4-5 level. The contrast and sharpness of the CSF-cord interface (arrowheads) are downgraded to grade 3 because of the interpolation process. The hydrated disks are hypointense and easily distinguished from the vertebrae. The boundaries of the neural foramina are well defined, but contrast between the exiting nerve roots and surrounding tissues is limited.

conditions on the basis of the tissue T1 and T2 and the choice of TR and TF (11).

Incorporation of a fast SE readout allows effective recovery of longitudinal magnetization to begin only after the last 180° radio-frequency pulse of the echo train, which reduces the time allowed for recovery (time for recovery of longitudinal magnetization = TR − [TF × ES]) (19). Recovery of longitudinal magnetization during a specific time period is dependent on the T1 of a particular tissue. If TR − (TF × ES) is more than four or five times T1 of a particular tissue, then complete recovery of longitudinal magnetization is expected. If, on the other hand, TR − (TF × ES) is less than four or five times T1 of a particular tissue, then incomplete recovery of longitudinal magnetization will occur, which results in a new steady-state longitudinal magnetization.

The transverse magnetization at the end of the echo train is proportional to $e^{-(TF \times ES)/T2}$. This monoexponential decay results in nearly complete loss of transverse magnetization when TF × ES is more than four or five times T2 of a particular tissue.

Implementation of the driven equilibrium pulse at the end of the echo train influences the recovery of longitudinal magnetization only when two conditions are met: (*a*) TR − (TF × ES) is less than four or five times T1, and (*b*) TF × ES is less than four or five times T2 of a particular tissue (16). The second condition is critical for achieving high signal from CSF at short TRs. Because of the relatively long T2 of CSF, the residual transverse magnetization of CSF is significantly greater at the end of a long echo train than that of other components of the cervical spine.

On the basis of results of simulations, increased SI from the cord can be achieved with longer TRs at the expense of longer acquisition times. We did not test imaging at longer TRs because the image quality was deemed by experienced observers (E.R.M., R.I.) to be satisfactory at TR of 211 msec. The fast SE pulse sequence used at MR imaging of the cervical spine in the five volunteers provided myelographic contrast at low TR (211 msec). The appearance of the remaining components of the cervical spine was more suggestive of T1 weighting.

These complex contrast characteristics have advantages and disadvantages. Because of the low SI of a hydrated disk with this pulse sequence, we expect delineation of acutely herniated disk fragments will be superior to that with either
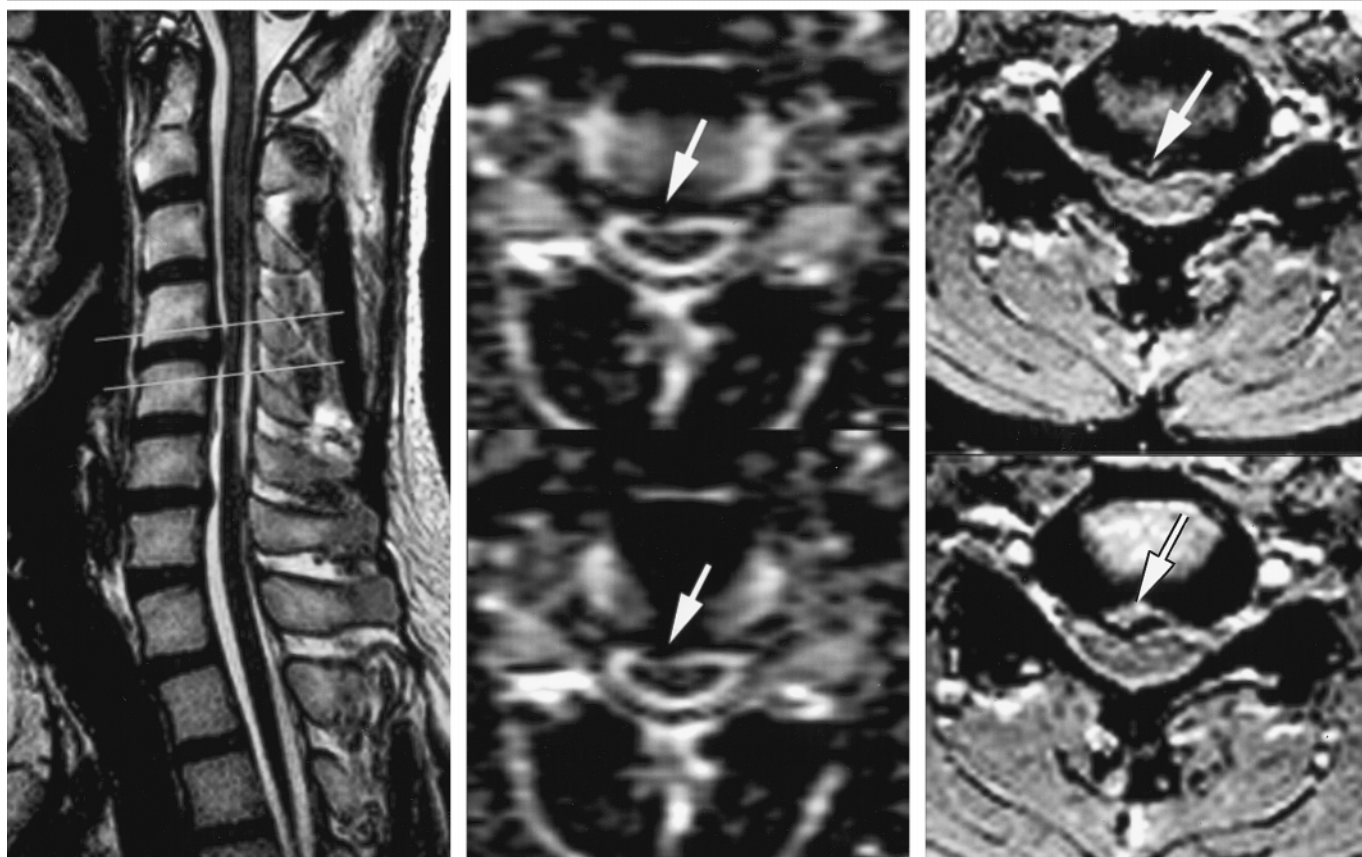
a. b. c.

Figure 4. Known degenerative disease of the cervical spine in a 40-year-old asymptomatic male volunteer. **(a)** Right parasagittal 3D fast SE MR image (211/60 [effective]) of the cervical spine was acquired with the driven equilibrium pulse. **(b)** Transverse 1-mm-thick contiguous reformatted MR image was obtained at the C4-5 level. **(c)** Transverse 1.5-mm-thick contiguous 3D gradient-echo MR images (30/12 with 5° flip angle) were obtained at the same level as in **b**. In **a** and **b**, a right paracentral disk or osteophyte (arrows in **b**) is easily distinguished from adjacent vertebral bodies, CSF, and cord. In **c**, however, the right paracentral disk or osteophyte (arrows) is more prominent (probably exaggerated), and the myelographic effect is poorly maintained (grade 1). In **b** and **c**, note slight degradation owing to the interpolation process.

TABLE 2
Mean Signal-to-Noise Ratio (SNR) from Different Tissues of the Cervical Spine before and after Application of Driven Equilibrium Pulse (DEP)

Tissue	SNR*		Ratio of SNR before DEP to SNR after DEP
	Before DEP	After DEP	
CSF	16.91 ± 2.75	80.40 ± 3.90	4.75
Cord	20.80 ± 0.74	17.79 ± 0.65	0.86
Disk	14.33 ± 0.76	10.86 ± 0.81	0.76
Bone Marrow	37.91 ± 3.53	31.88 ± 2.77	0.84

* Data are the mean SNR plus or minus SD.

T1- or T2-weighted sequences. On the other hand, differentiation between disk fragment and osteophyte may be difficult. Because the anterior approach is the surgical treatment chosen most often in spondylotic disease of the cervical spine, differentiation of disk from osteophyte is less critical.

The limited contrast in the neural foramina may lessen the conspicuity of lateral disk herniations and their relationship to the exiting nerve roots. Administration of T1-shortening agents may improve contrast in the neural foramina (20). The performance of this pulse sequence remains uncertain with regard to demonstration of spinal cord abnormalities. We expect that the driven equilibrium pulse will render long T2 lesions hyperintense to cord. Further clinical experience is needed to answer this question.

Shortening of the TR permitted 3D single-slab sagittal MR imaging of the cervical spine that is clinically applicable and nearly isotropic, with enough left-to-right coverage to allow quality transverse reformatted images. Single-slab sagittal MR imaging eliminates the slab-boundary artifacts commonly encountered on transverse reformatted images generated with multislab techniques (21,22). Also, isotropic voxel imaging allows quality reformatted images in any plane. The imaging voxel is nearly isotropic with the pulse sequence evaluated in this study, because the partition thickness is reduced from 2 to 1 mm by means of interpolation in the section-select direction (zero filling) (2). The interpolation process may slightly degrade the transverse reformatted images.

The TF and range of TF × ES (96.0–113.6 msec) dictated by our choice of sequence parameters can be altered by changing the effective echo time and the type of trajectory used to fill k space. For a given TR and k-space trajectory, the choice of a shorter effective echo time results in a decrease in TF and a lower (not necessarily tighter) range of TF × ES, which leads to improvement in myelographic contrast (Fig 2) but longer acquisition times.

These computer-generated data are limited and can serve as only general guidelines for pulse sequence development. Limitations in this study include (*a*) the use of approximations to derive the simplified equation that quantified the effect of the driven equilibrium pulse on steady-state SI (16), (*b*) the use of approximate T1 and T2 for the spinal cord by averaging the relaxation times of gray and white matters, and (*c*) discounting of the effect of CSF pulsation on contrast calculation.

In conclusion, addition of the driven equilibrium pulse to the end of a 3D fast SE MR pulse sequence provides strong myelographic contrast at short TRs. On the basis of results of computer simulations that account for the effect of the driven equilibrium pulse, we describe a single-slab 3D fast SE MR imaging sequence that is time efficient and nearly isotropic and may prove useful for evaluation of the degenerative cervical spine.

References
1. Georgy BA, Hesselink JR. MR imaging of the spine: recent advances in pulse sequences and special techniques. AJR Am J Roentgenol 1994; 162:923–934.
2. Ross JS. Newer sequences for spinal MR imaging: smorgasbord or succotash of acronyms? AJNR Am J Neuroradiol 1999; 20:361–373.
3. Enzmann DR, Rubin JB, Wright A. Cervical spine MR imaging: generating high-signal CSF in sagittal and axial images. Radiology 1987; 163:233–238.
4. Enzmann DR, Rubin JB. Cervical spine: MR imaging with a partial flip angle, gradient-refocused pulse sequence. I. General considerations and disk disease. Radiology 1988; 166:467–472.
5. Szeverenyi NM, Kieffer SA, Cacayorin E. Correction of CSF motion artifact on MR images of the brain and spine by pulse sequence modification: clinical evaluation. AJNR Am J Neuroradiol 1988; 9:1069–1074.
6. Haacke EM, Wielopolski PA, Tkach JA, Modic MT. Steady-state free precession imaging in the presence of motion: application for improved visualization of the cerebrospinal fluid. Radiology 1990; 175:545–552.
7. Zur Y, Wood ML, Neuringer L. Motion-insensitive, steady-state free precession imaging. Magn Reson Med 1990; 16:444–459.
8. Wood ML, Zur Y, Neuringer L. Gradient moment nulling for steady-state free precession MR imaging of cerebrospinal fluid. Med Phys 1991; 18:1038–1044.
9. Czervionke LF, Daniels KL, Wehrli FW, et al. Magnetic susceptibility artifacts in gradient-recalled echo MR imaging. AJNR Am J Neuroradiol 1988; 9:1149–1155.
10. Tsuruda JS, Remley K. Effects of magnetic susceptibility artifacts and motion in evaluating the cervical neural foramina on 3DFT gradient-echo MR imaging. AJNR Am J Neuroradiol 1991; 12:237–241.
11. Sze G, Kawamura Y, Negishi C, et al. Fast spin-echo MR imaging of the cervical spine: influence of echo train length and echo spacing on image contrast and quality. AJNR Am J Neuroradiol 1993; 14:1203–1213.
12. Oshio K, Jolesz FA, Melki PS, Mulkern RV. T2-weighted thin-section imaging with the multislab three-dimensional RARE technique. J Magn Reson Imaging 1991; 1:695–700.
13. Tsuruda JS, Norman D, Dillon W, Newton TH, Mills DG. Three-dimensional gradient-recalled MR imaging as a screening tool for the diagnosis of cervical radiculopathy. AJR Am J Roentgenol 1990; 154:375–383.
14. Melhem ER, Benson ML, Beauchamp NJ, Lee RR. Cervical spondylosis: three-dimensional gradient-echo MR with magnetization transfer. AJNR Am J Neuroradiol 1996; 17:705–711.
15. Constable RT, Gore JC. The loss of small objects in variable TE imaging: implications for FSE, RARE, and EPI. Magn Reson Med 1992; 28:9–24.
16. van Uijen CMJ, Den Boef JH. Driven-equilibrium radiofrequency pulses in NMR imaging. Magn Reson Med 1984; 1:502–507.
17. Mugler JP III, Spraggins TA, Brookeman JR. T2-weighted three-dimensional MP-RAGE MR imaging. J Magn Reson Imaging 1991; 1:731–737.
18. Rydberg JN, Riederer SJ, Rydberg CH, et al. Contrast optimization of fluid-attenuated inversion recovery (FLAIR) imaging. Magn Reson Med 1995; 34:868–877.
19. Lee JN, Riederer SJ. A modified saturation-recovery approximation for multiple spin-echo pulse sequences. Magn Reson Med 1986; 3:132–134.
20. Ross JS, Ruggieri PM, Glicklich M, et al. 3D MRI of the cervical spine: low flip angle FISP vs. Gd-DTPA turbo FLASH in degenerative disk disease. J Comput Assist Tomogr 1993; 17:26–33.
21. Blatter DD, Parker DL, Robison RO. Cerebral MR angiography with multiple overlapping thin slab acquisition. I. Quantitative analysis of vessel visibility. Radiology 1991; 179:805–811.
22. Robison RO, Blatter DD, Parker DL, et al. Reduction of slab boundary artifact with multiple overlapping thin slab acquisition in MR angiography of the cervical carotid artery. J Magn Reson Imaging 1994; 4:529–535.